J Appl Electrochem (2008) 38:985–992
DOI 10.1007/s10800-008-9511-9

ORIGINAL PAPER

Development of gel-polymer electrolytes and nano-structured electrodes for Li-ion polymer batteries

C. Gerbaldi · J. Nair · C. Bonatto Minella · G. Meligrana · G. Mulas · S. Bodoardo · R. Bongiovanni · N. Penazzi

Received: 15 September 2007 / Revised: 1 February 2008 / Accepted: 1 February 2008 / Published online: 21 February 2008

Abstract A novel methacrylic gel-polymer membrane was synthesized by free radical photo polymerisation (UV-curing technique). The polymerisation was very easy, fast and reliable and the membrane shows good behaviour in terms of both conductivity and cyclability in Li cells. The anode materials were prepared by high energy ball milling obtaining nanocrystalline Ni–Sn alloys, while the hydrothermal processing in presence of a template was used to prepare nanostructured $LiFePO_4$/C as cathode material. Every component has been characterised separately from the structural and electrochemical point of view. The first experimental data on the performance of a complete Li-ion polymer cell assembled with the components studied are also presented. The results obtained demonstrate the overall satisfying, and some superior performances of the various single components and their feasibility as a complete system.

Keywords Methacrylic-based gel-polymer electrolyte · UV-curing · Nanostructured electrode · Ni–Sn alloy · Lithium iron phosphate · Li-ion polymer battery

C. Gerbaldi (✉) · J. Nair · G. Meligrana · S. Bodoardo · R. Bongiovanni · N. Penazzi
Department of Materials Science and Chemical Engineering, Politecnico di Torino, C.so Duca degli Abruzzi 24, 10129 Turin, Italy
e-mail: claudio.gerbaldi@polito.it

C. B. Minella · G. Mulas
Department of Chemistry, University of Sassari, via Vienna 2, 07100 Sassari, SS, Italy

1 Introduction

In the field of consumer electronics and automotives, the constant demand for higher energy density, thinner, lighter and even more mechanically flexible batteries, which are safe and low cost, has motivated research into new suitable materials, both electrodes and electrolytes, for secondary Li-ion batteries [1–3].

High performing innovative materials are important for all the components of a Li-ion cell. The electrode materials need to have high capacity and durability, while the electrolyte should be a solid membrane capable of high ionic conductivity even at ambient temperature, with good mechanical and interfacial properties and stable performances. In all cases the materials must be low cost, ecologically friendly and safe.

As polymer electrolyte, a novel methacrylic-based membrane was synthesized and its characteristics were evaluated. The method adopted for preparing the gel-polymer electrolyte was free radical photo polymerisation (UV-curing), which is a well-established polymerisation technique, taking place at room temperature under UV light [4]. The potentials of this technique, commonly employed for the preparation of coatings and inks and for the production of optical and electronic devices, can be diverted to our field of interest [5] to obtain very fast, low-cost production and to have an environmentally friendly approach, as the use of solvents is almost avoided. In fact, highly cross-linked polymers are readily synthesized by irradiation of the appropriate formulation of multifunctional monomers, namely acrylates and methacrylates, in the presence of a photo initiator [6].

Nanostructured materials, in view of their application as cathodes and anodes, have also been investigated. As for the anode, our attention turned to the Ni–Sn binary system,

for which literature data suggested interesting electrochemical properties [7–10]. These arise from the coupling of the specific role of the Sn phase, which is active to the Li^+ intercalation, and the role of Ni as a "matrix", able to assist the volume expansion during the lithiation process. For the synthesis of these alloys we used the ball-milling technique, which is recognised as a powerful mechanical processing tool for the preparation of a variety of metastable materials, including nanostructured as well as amorphous and quasi-crystalline phases. The hydrothermal process in the presence of an organic surfactant (CTAB) has been used to prepare nanostructured $LiFePO_4$ as cathode material. An easy, quick and low cost hydrothermal synthesis was developed leading to the preparation of high surface area and high performing phospho-olivine powders [11].

The aim of the present contribution is to show the initial developments of the aforementioned components regarding their structural–morphological characteristics and electrochemical performance. In addition, the preliminary testing of a laboratory prototype of a complete Li-ion polymer cell is presented.

2 Experimental

2.1 Synthesis

The polymeric membrane was obtained by UV-curing a reactive mixture of Bisphenol A ethoxylate (15 EO/phenol) dimethacrylate (BEMA, $M_n = 1700$, Aldrich) and poly(ethylene glycol) methyl ether methacrylate (PEGMA, $M_n = 1100$, Aldrich), in 70:30 ratio, in the presence of 2 wt% of free radical photo-initiator (Darocur 1173, Ciba Specialty Chemicals). The curing procedure is fully described by Nair et al. [6]. The curing was carried out on the preformed monomers mixture, diluted with a 1:1 w/w ethylene carbonate and diethyl carbonate solution (EC-DEC, Fluka) in the 55:45 ratio. The membrane, around 200 μm thick, was further swelled in 1.0 M $LiPF_6$ in 1:1 w/w EC/DEC solution (Selectipur LP 40, Merck) for two hours. Overall, this process usually takes less than 3 hrs for the production of transparent and flexible gel-polymer membranes. All the above reported procedures were performed in the inert atmosphere of an Ar-filled dry glove box (MBraun Labstar, O_2 and H_2O content <0.1 ppm).

The mechanochemical synthesis of intermetallic Ni–Sn alloys was carried out by ball milling using a SPEX Mixer-Mill Model 8000 equipped with stainless-steel vial and spheres. Elemental powders of Ni (Sigma-Aldrich, 100 mesh, 99.99%), Sn (Mattey Reagent, 325 mesh, 99.8%) and graphite (Aldrich, 99.5%) were used, and the vial was charged with 8.0 g powder mass and two balls of 8.0 g each. To avoid oxidation, vial charging and sampling were performed in the Ar-filled dry glove box. Various nominal compositions were selected and synthesized, the one considered in this paper is $Ni_{44}Sn_{56}$ (expressed in atomic percentage). The alloy was prepared in two different ways. In the first case, by milling only the pure metals; while, in the second, grinding pure Ni and Sn with 10 wt% of graphite, to overcome the addition stage of electronic conductor during the electrode preparation. In all cases, the final powder samples was further ground in an agate mortar in the dry box and finally sieved with a 75 μm molecular sieve.

The nanostructured $LiFePO_4$ powders were prepared by direct mild hydrothermal synthesis. Starting materials were $FeSO_4 \cdot 7H_2O$ (Aldrich, purity 99%), H_3PO_4 (Aldrich, purity >85%), LiOH (Aldrich, purity >98%) in the stoichiometric ratio 1:1:3 and hexadecyltrimethylammonium bromide (Aldrich, $C_{19}H_{42}BrN$, CTAB). The detailed synthesis procedure is reported in Meligrana et al. [11].

2.2 Analyses and characterisation techniques

The characterisation of the UV-cured film included the determination of the gel content, dynamo-mechanical and thermo-gravimetric analysis [6, 12].

Structural characterisation of the anode materials was performed by XRD, employing a Rigaku DMax diffractometer equipped with Cu-Kα radiation and a graphite monochromator in the diffracted beam. The diffraction data were collected in the 2θ-range between 20 and 80°, with an acquisition step of 0.05° and a time per step of 10 sec. Quantitative evaluation of phase abundance, as well as the estimation of the average crystallite size and the average lattice strain content, were studied by employing least squares based fitting profile refinement procedures, according to the Rietveld method. The lattice strain content, which is a-dimensional, is also referred to as root mean square micro-strain, and it is defined as the ratio between lattice distortion amplitude and interplanar distance as a consequence of an applied stress.

The characterisation of nanostructured $LiFePO_4$ powders included quantitative elemental analysis and structural–morphological investigation as described in [11].

2.3 Electrodes and cell preparation, electrochemical characterisation techniques

The ionic conductivity of the gel polymer membrane was determined by electrochemical impedance spectroscopy (EIS); its electrochemical stability window was evaluated

by running sweep voltammetry in a 2-electrode Teflon cell. A full description of these experimental procedures is reported in [6].

Both the Ni–Sn and the $LiFePO_4$-based electrodes were prepared in the form of thin films by casting on a copper or aluminium current collector, respectively, a N-methyl-2-pyrrolidone (NMP, Aldrich) slurry of the active material mixed with acetylene black as electronic conductor (Shawinigan Black AB50, Chevron Corp., USA) and poly(vinylidene fluoride) as binder (PVdF, Solvay Solef 6020). The composite electrodes were tested in three electrodes polypropylene T-type cells with Li metal as both the counter and the reference electrodes. A glass-wool (Whatman GF/A) disc was used as the separator. The liquid electrolyte used was 1.0 M $LiPF_6$ in a 1:1 mixture of ethylene carbonate (EC) and diethyl carbonate (DEC).

The Ni_3Sn_4 composite electrode was prepared by blending 82 wt% alloy powder, 10 wt% carbon black, and 8 wt% PVdF; while the Ni_3Sn_4–C composite electrode was prepared by blending 92 wt% active material, 0 wt% carbon black, and 8 wt% PVdF. The coatings were then dried in air at 60 °C. The electrodes, which had an area of 0.785 cm^2, were cycled galvanostatically at room temperature and at different current rates, ranging from C/10 to 1C, between 0.02 and 1.20 V vs. Li. The $LiFePO_4$/C composite electrode was prepared and cycled as reported in Meligrana et al. [11].

The Li-ion polymer cell laboratory prototype was assembled by laminating the three components in sequence, i.e. the NiSn-based anode film, a layer of the gel-polymer electrolyte and the $LiFePO_4$-based cathode film. This assembly was housed in a Teflon-made Swagelok cell equipped with two stainless steel current collector electrodes.

Both electrode fabrication and cell assembly were performed in the environmentally controlled Ar-filled dry glove box. The characteristics and performance of both Li and Li-ion cells were investigated at room temperature in terms of charge/discharge cycling at different current regimes by an Arbin Instrument Testing System model BT-2000.

3 Results and discussion

3.1 UV-cured methacrylic membranes as gel-polymer electrolyte

The gel-polymer electrolyte (namely, BMPE) is based on a transparent freestanding and non-tacky although extremely flexible membrane obtained by copolymerising the monomers BEMA and PEGMA via UV irradiation. BEMA, being a di-functional monomer, forms a highly cross-linked network that can be swelled by the liquid electrolyte and can efficiently hold it. PEGMA, which acts as a reactive diluent and is incorporated into the network, was used because it has a long and flexible ethoxy chain which can improve the mobility of Li^+ ions inside the polymer matrix [1, 13–16]. PEGMA also reduces the cross-linking density and the *T*g of the membranes.

The percentage of acrylic double bond conversion at the end of the UV irradiation was evaluated from kinetic studies (real-time FT-IR). It shows that the reactivity was very high and a quantitative yield (i.e. >98%) is obtained in approx. 80 s. The gel content, which represents the percentage of materials insoluble in chloroform, is 98.9%; this means that the membrane is a highly cross-linked thermoset material, in good agreement with the conversion results obtained by the kinetics studies. From the DMTA spectra, the *T*g, detected as the maximum of tan δ peak, was found to be −49 °C; this indicates that at room temperature the polymer is in a rubbery state. Finally, the membrane showed a high thermal stability up to 300 °C.

The membrane containing the EC-DEC solution and swelled by the liquid electrolyte solution after UV-curing was still non-tacky, transparent and, as expected, extremely flexible. It showed a temperature stability up to 130 °C, when the solvents began to evaporate. This result indicates that the gel-polymer membrane can be safely used in Li-ion polymer batteries up to 100 °C.

In view of its possible application as electrolyte in Li-ion polymer batteries, BMPE was tested in terms of its general electrochemical properties. The ionic conductivity was evaluated by impedance spectroscopy and the Arrhenius plot is shown in Fig. 1. The ionic conduction in gel-polymer electrolytes follows the VTF (Vogel-Tamman-Fulcher) relation [17–20] which describes the transport properties in a viscous matrix. At sufficiently high

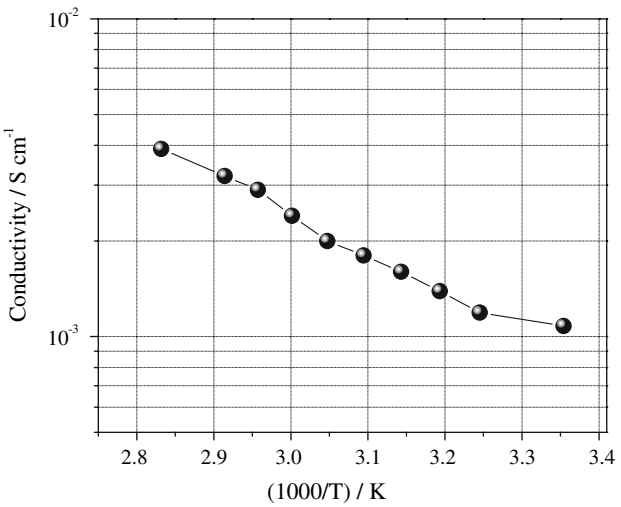

Fig. 1 Conductivity versus temperature plot of BMPE gel-polymer membrane. Data obtained by impedance spectroscopy

temperatures, as in our case, the VTF behaviour approaches Arrhenius behaviour. The membrane showed 1.1 × 10^{-3} S cm^{-1} at room temperature, which is almost comparable with those of common Li-ion liquid electrolytes. The ionic conductivity increased with increase in temperature, resulting in 3.9 × 10^{-3} S cm^{-1} at 80 °C.

The electrochemical stability at potential values anodic with respect to lithium was evaluated at room temperature. The current-voltage curve, reported in Fig. 2, was obtained for a working Super-P electrode swept in a cell using the gel electrolyte membrane and a lithium metal counter electrode. The onset of the current, which is representative of the decomposition of the electrolyte, indicates an anodic break-down voltage of approx. 4.8 V vs. Li (the cathodic sweep limit value is found to be around 0.0 V vs. Li, with flat profile and very low residual current towards the whole voltage range). Such a high decomposition voltage is certainly welcome for practical application [14, 21]. The anodic scan showed very low residual current prior to breakdown voltage, confirming the purity of the prepared membrane and the synthesising method adopted, because the system as a whole is sensitive to oxygen, water and other impurities.

3.2 Anodes: nanocrystalline Ni–Sn alloy obtained by high energy ball milling

Among the various Ni–Sn intermetallic compounds prepared using high energy ball-milling, the investigations done by our research group have found that the mixture with atomic composition $Ni_{44}Sn_{56}$ which, according to the equilibrium binary phase diagram, forms the monoclinic Ni_3Sn_4 intermetallic phase [JCPDS #040851], is the best performing anode material. As reported in the experimental section, a sample was also prepared by adding graphite during ball-milling to optimise the milling conditions, keeping in mind that such additive could improve the conductivity of the material more efficiently than the acetylene black which is added during the electrode preparation.

The XRD patterns of the Ni_3Sn_4 intermetallic phase, prepared both with and without the addition of graphite during ball-milling, are shown in Fig. 3 (as patterns a and b). Structural and microstructural features of the as-prepared powders, as well as the time of treatment, depended on the reagent stoichiometry and relative data are collected in Table 1. While the micro-strain content was similar, slightly smaller average crystalline sizes pertained to the Ni_3Sn_4–C sample, obtained with longer mechanical treatment time.

Addition of C during the milling stage did not change the nanostructural features of the resulting Ni_3Sn_4–C alloy. The small variation observed in the lattice parameters suggests that only a negligible amount of graphite diffused within the nanostructured intermetallic domains. In contrast, as shown by the SEM investigation reported in Fig. 4, the presence of graphite modifies the overall morphology of the grains; in particular, it limits the particle aggregation leading to a considerable decrease in size.

Figure 5 shows the discharge and charge profiles of the electrodes upon cycling in a Li cell at C/10 rate. The

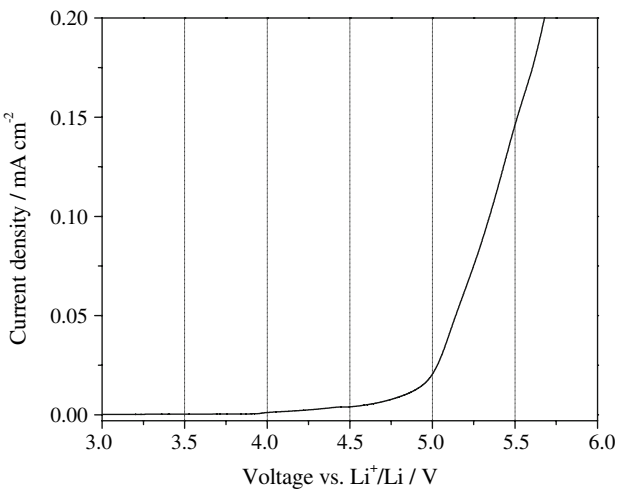

Fig. 2 Current–voltage curves at 25 °C of the BMPE gel-polymer membrane. Cell configuration adopted: Super-P carbon over aluminium current collector as working electrode, Li metal as counter electrode and the given membrane as electrolyte. Anodic potential scan range from O.C.V to 6.0 V vs. Li at 0.100 mV s^{-1}

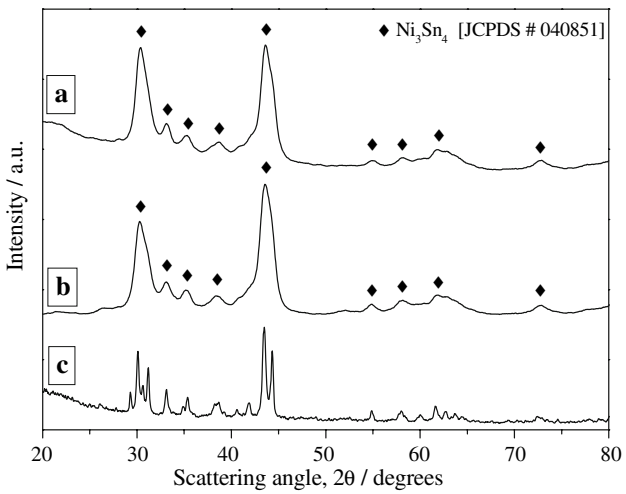

Fig. 3 XRD patterns of (a) Ni_3Sn_4–C and (b) Ni_3Sn_4 alloys after 50 and 70 h milling, respectively. Pattern (c) crystalline Ni_3Sn_4 obtained after heat-treating at 600 °C in high purity inert Ar atmosphere the nanostructured Ni_3Sn_4 intermetallic phase of pattern (b): narrow peaks belong to the Ni_3Sn_4 crystalline phase. Diagonal symbols represent the Ni_3Sn_4 theoretical Bragg reflections according to [JCPDS # 040851]

Table 1 Structural and microstructural features of the as-prepared nanocrystalline alloy powders

Nominal composition	Milling time/hours	Crystallite avg size/Å	Micro-strain $*10^{-3}$	Cell parameter/Å
$Ni_{44}Sn_{56}$	50	151	5.6	a = 12.462
				b = 4.101
				c = 5.219
				β = 103.94
$Ni_{44}Sn_{56}$–C	70	144	4.0	a = 12.488
				b = 4.103
				c = 5.218
				β = 104.11

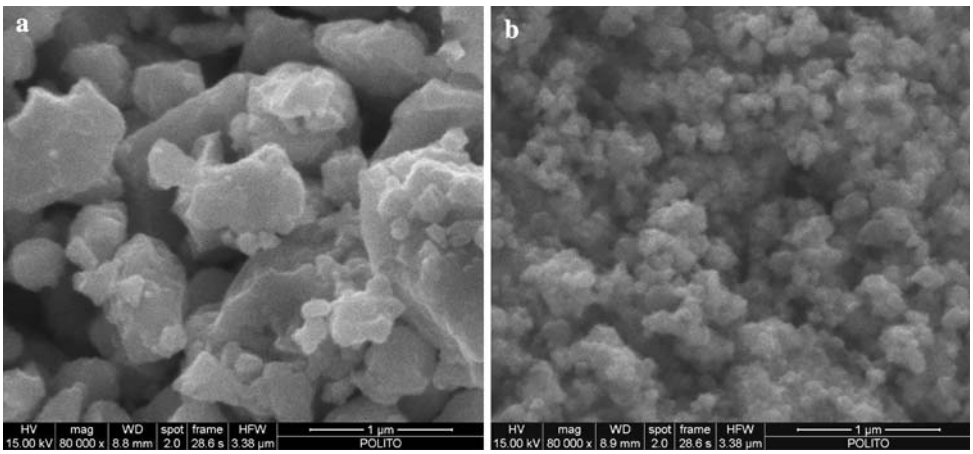

Fig. 4 SEM images of (**a**) Ni_3Sn_4 and (**b**) Ni_3Sn_4–C alloy sieved powders

behaviour is similar to that reported for Ni_3Sn_4 by Amadei et al. [7]. In particular, the first discharge (lithium alloying) curve shows a typical shoulder around 0.70 V vs. Li, an irreversible process which is due to both the formation of $Li_{4.4}Sn$ alloy and the decomposition of solvent, with the formation of a passivating film on the electrode surface. The charge curves also show the same characteristic S-type shape, centred at an average voltage of about 0.45 V vs. Li for the lithium de-alloying reversible electrode process. The specific capacity associated with the subsequent cycles is about 40% less than that of the first discharge.

The specific capacity for Ni_3Sn_4–C is detectably higher than that of Ni_3Sn_4. This feature is clearly evident in Fig. 6, which shows the comparison between the cycling behaviour of the two samples at room temperature (current regimes ranging from C/10 to 1C). At almost all cycling regimes, the specific capacity of Ni_3Sn_4–C is about 30% higher than Ni_3Sn_4. Though the performances of both the samples are far below the theoretical value of 725 mAh g^{-1}, this finding is important because it shows the marked positive effect of the graphite added during sample preparation. It is easy to draw the conclusion that addition of graphite during ball-milling improves contact between the conduction enhancer and the active material grains. As already reported, SEM micrographs in Fig. 4 suggest that

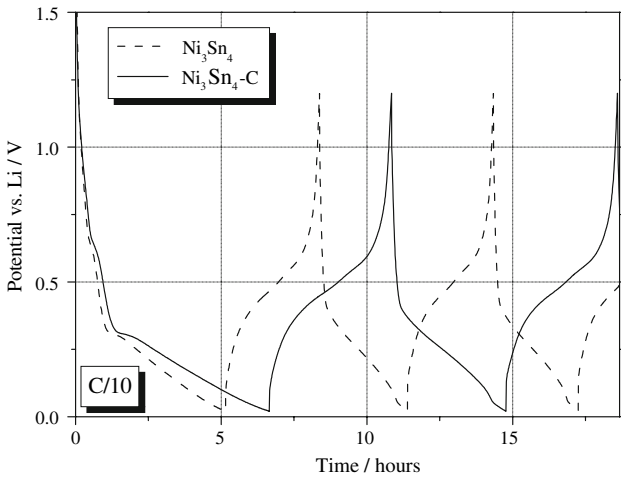

Fig. 5 Room temperature electrochemical voltage profile of Ni_3Sn_4 (dash line) and Ni_3Sn_4–C (solid line) alloys, cycled between 1.20 and 0.02 V vs. Li at C/10 rate

graphite extends its positive influence, even to the particle morphology and dimensions.

Figure 7 shows the durability of the Ni_3Sn_4–C electrode upon prolonged cycling at room temperature (C/5 rate, approx. 1.0 mA cm^{-2}). After the initial loss already discussed, the specific capacity is quite stable with a highly

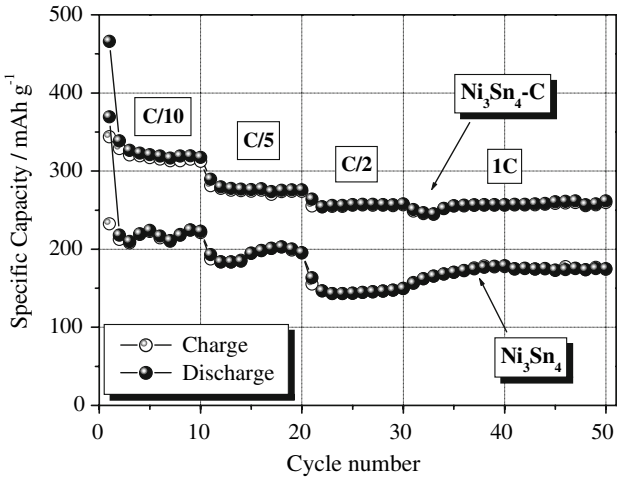

Fig. 6 Room temperature cycling performances of Ni_3Sn_4 and Ni_3Sn_4–C alloys at C-rates ranging from C/10 to 1C. Discharge = Li alloying, charge = Li de-alloying

reversible charge/discharge capacity above 250 mAh g^{-1} and an almost negligible fade within the initial 100 cycles.

3.3 Cathode: nanostructured $LiFePO_4$/C by hydrothermal synthesis

Phospho-olivine lithium iron phosphate ($LiFePO_4$) is among the most promising candidates for the next-generation of Li-ion battery cathodes [22–24]. It shows several advantages compared to conventional cathode materials, namely lower toxicity and cost. In addition, $LiFePO_4$ has an interesting theoretical specific capacity of about 170 mAh g^{-1}, a good cycle stability and a technically attractive flat voltage versus current profile of 3.45 V vs. Li^+/Li, due to the two-phase extraction/insertion mechanism. Unfortunately, it also has two main drawbacks, i.e. poor diffusion of lithium through the $LiFePO_4/FePO_4$ interfaces and poor electronic conductivity arising from corner-shared FeO_6 octahedra with a large charge transfer gap and lack of mixed valency (two-phase reaction) [25].

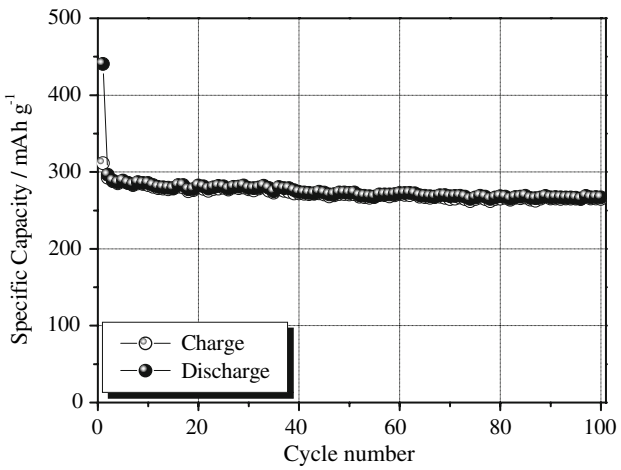

Fig. 7 Specific capacity vs. cycle number for the Ni_3Sn_4–C alloy (C/5 rate ≅ 1 mA cm^{-2}, room temperature). Discharge = Li alloying, charge = Li de-alloying

In order to overcome these major limitations, we developed a new, easy and low-cost mild hydrothermal synthesis which resulted in a nano-structured $LiFePO_4$/C with high specific surface area and electrochemical performances [11]. The synthesis was performed in the presence of an organic surfactant compound (CTAB), under autogenously pressure in a Teflon-lined stainless steel autoclave. The use of CTAB is critical in our method in several ways. As a surfactant, it functions as a dispersing agent which limits the nucleation and growth of large crystallites, thus leading to the formation of nano-sized particles (enhancement in Li^+-ion diffusion). It also acts as internal reducing agent, thus limiting the formation of Fe^{3+} species and increasing the purity degree of the sample. Moreover, due to the complexing nature of the polar heads of the micelles with Fe ions, CTAB also remains close to the surface of the crystallites after filtration and, during the firing in inert atmosphere, it gives rise to a carbon coating that increases the electronic conductivity of the material.

The method resulted in a highly homogenous nano-structured $LiFePO_4$/C, with a high specific surface area of 44.70 m^2 g^{-1} and an extremely low content of secondary phases. The expected $LiFePO_4$ stoichiometry is obtained: the molar ratio for Li:Fe:P is almost 1:1:1. As for carbon, the content is 4.80 wt%.

From a structural viewpoint, the Rietveld refinement gives results with a good residual factor (see Fig. 8). The refinement data show that the main phase is represented by $LiFePO_4$ (orthorhombic, s.g. *Pnma*), and show extremely good correspondence with the reference $LiFePO_4$ pattern [26, 27]. The sample appears well-crystallised and almost perfectly single phase. In fact, the fitting between calculated and measured data is very good and only minor α-Fe impurities (less than 1%) are detectable.

A good estimation of the average crystalline domain size (D) has been calculated from Scherrer's equation and the results are reported in Table 2, which points out the nano-crystallinity of the synthesized material. The refined lattice parameters correspond almost perfectly to the precise results of Streltsov et al. [26], differing from the single-crystal data by less than 1.00‰. This is only because of the different degree of crystallization between the powder and the single-crystal synthesis.

HR-TEM analyses are reported in Fig. 9 and confirm the fundamental role of CTAB in the synthesis of the samples. All the solid consists of pure $LiFePO_4$ particles, with an average size of 20–30 nm. Secondary phases and/or

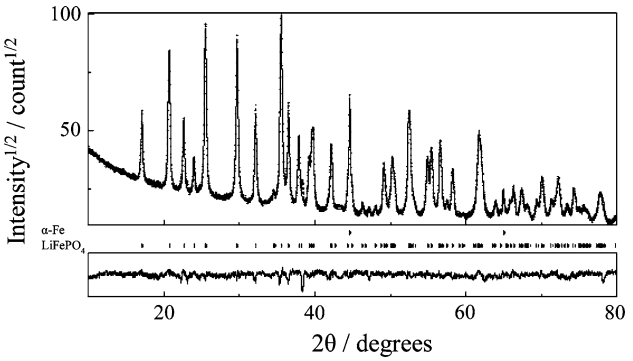

Fig. 8 Results of the Rietveld refinement on the X-ray powder diffraction pattern of nanostructured $LiFePO_4$/C. See text for the discussion

Table 2 Refined lattice parameters, in comparison with those taken from the literature [22], and average crystalline domain size (D) of the nano-crystalline $LiFePO_4$/C powder

	a/Å	b/Å	c/Å	Volume/Å^3	D/nm
Single crystal	10.332	6.010	4.692	291.351	–
$LiFePO_4$/C	10.328	6.003	4.700	291.395	32

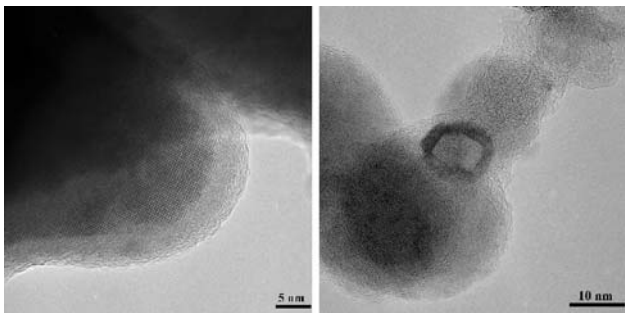

Fig. 9 HR-TEM analysis of nanocrystalline $LiFePO_4$/C

impurity particles are not observed. Pure and perfectly crystallized $LiFePO_4$ particles are small and covered with a very homogeneous layer of carbon, approximately 5 nm thick. Some particles are even completely embedded in carbon.

As a result, the synthesized material shows very interesting electrochemical performances. This is shown in Fig. 10 which reports the cycling performance of a $LiFePO_4$/C electrode at RT at the C-rate C/20 to 20C in liquid electrolyte. The plot shows the high specific capacity and the good cycling stability of this material, which has a high rate capability and even a slight progressive improvement of the charge coefficient with increasing applied current density. The performance is good, particularly at high discharge regimes, which is very important for high power applications. In fact, the sample still maintains the 65% of the theoretical capacity at very high current regime of 20C.

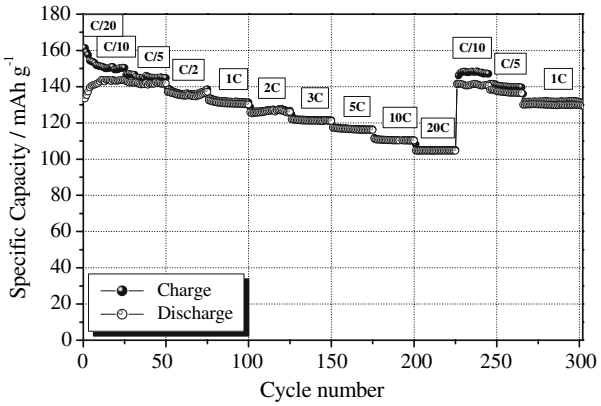

Fig. 10 Room temperature charge–discharge cycling test of $LiFePO_4$/C electrode at different C-rate (from C/20 to 20C). 1.0 M $LiPF_6$ in 1:1 w/w EC:DEC solution has been used as the electrolyte

3.4 Assembly and preliminary investigation of a Li-ion polymer cell

In view of the possible practical application of these nanostructured electrodes and gel-polymer electrolyte, they were assembled in a complete Li-ion polymer battery laboratory prototype, and its electrochemical behaviour was investigated by means of galvanostatic charge/discharge cycling. The response of the prototype, assembled by combining the Ni_3Sn_4–C anode with the $LiFePO_4$/C cathode and using the BMPE membrane as the separator, is reported in Fig. 11(a,b). Figure 11(a) shows some typical voltage vs. time profiles, obtained at room temperature at approx. C/10 rate with respect to $LiFePO_4$. The battery

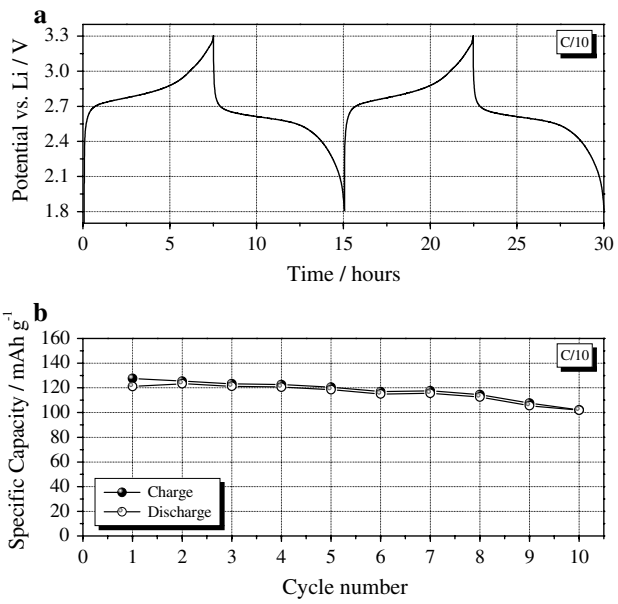

Fig. 11 Room temperature charge/discharge voltage vs. time profiles (3rd and 4th cycles) (**a**) and specific capacity vs. cycle number (**b**) of Ni_3Sn_4–C/ BMPE membrane/ $LiFePO_4$/C Li-ion cell, cycled at about C/10 rate vs. $LiFePO_4$

operating voltage was around 2.8 V, reflecting the electrochemical process of lithium cycling transfer from the cathode to the anode [28]:

$$Sn + LiFePO_4 \leftrightarrows Li_xSn + Li_{(1-x)}FePO_4.$$

The voltage difference between the charge and discharge level, some 0.250 V, is probably related to the electrolyte, to the contact resistance at the electrode-electrolyte interface and to the anode behaviour. Since the battery is cathode limited, its maximum specific capacity is evaluated to be 169 mAh g^{-1} ($LiFePO_4$ theoretical capacity [22]).

Figure 11(b), which illustrates the cycling performance of the battery, shows that it can deliver approx. 125 mAh g^{-1} in the first cycle (i.e. approx. 75% with respect to the maximum possible value) which is in accord to the over-voltage detected. The cycling efficiency is high. Another positive feature is the repetitive shape of the cycles, reflected in the stable trend of the capacity curve. The actual prototype battery suffers from capacity loss over cycling (after ten cycles the specific capacity fades to approx. 100 mAh g^{-1}). This aspect is under additional investigation in our labs and questions still remain on the capacity retention upon prolonged cycling.

4 Conclusions

All the Li-ion battery components developed in the present work show common features: eco-compatibility, low cost and ease of preparation. The preliminary results indicate that UV-curing is a suitable method for synthesizing membranes for use as gel-polymer electrolyte for Li-ion batteries. Compared to other techniques, it appears highly advantageous due to its easiness and rapidity in processing. The copolymerisation process is fundamental to obtain gel-polymer electrolytes with high anodic breakdown voltage (>4.5 V vs. Li) and high ionic conductivity even at ambient temperature.

Though the actual results regarding Ni–Sn alloys are far from being optimised, the system has high potential (725 mAh g^{-1} is the theoretical specific capacity for Ni_3Sn_4), and much is still to be tried. $LiFePO_4$ is one of the most promising cathode materials and the literature in this subject is huge. The synthetic method presented here allows to a material with high electrochemical properties at the lowest cost to be obtained.

The results obtained by the Li-ion polymer cell assembled with the various components produced aims at demonstrating that the various materials are ready to be applied and optimised on an industrially interesting system.

Acknowledgements Financial support from the Italian Regione Piemonte Council (research project C116) is gratefully acknowledged.

References

1. Scrosati B (1995) Nature 373:557
2. Piana M, Arrabito M, Bodoardo S, D'Epifanio A, Satolli D, Croce F, Scrosati B (2002) Ionics 8:17
3. Scrosati B (2005) Chem Records 5(5):286
4. Decker C (1996) Prog Polym Sci 21:593
5. Song M, Cho J, Cho BW, Rhee H (2002) J Power Sources 110:209
6. Nair J, Gerbaldi C, Meligrana G, Bongiovanni R, Bodoardo S, Penazzi N, Reale P, Gentili V (2007) J Power Sources (in press). doi:10.1016/j.jpowsour.2007.08.004
7. Amadei I, Panero S, Scrosati B, Cocco G, Schiffini L (2005) J Power Sources 143:227
8. Mukaibo H, Sumi T, Yokoshima T, Momma T, Osaka T (2003) Electrochem Solid-State Lett 6(10):A218
9. Mukaibo H, Momma T, Mohamedi M, Osaka T (2005) J Electrochem Soc 152(3):A560
10. Ehrlich GM, Durand C, Chen X, Hugener TA, Spiess F, Suib SL (2000) J Electrochem Soc 147(3):886
11. Meligrana G, Gerbaldi C, Tuel A, Bodoardo S, Penazzi N (2006) J Power Sources 160:516
12. Sangermano M, Bongiovanni R, Malucelli G, Roppolo I, Priola A (2006) Prog Organic Coatings 57:44
13. Scrosati B, Croce F, Persi L (2000) J Electrochem Soc 147:1718
14. Croce F, Sacchetti S, Scrosati B (2006) J Power Sources 162:685
15. Lightfoot P, Metha MA, Bruce PG (1993) Science 262:883
16. Oh B, Jung W, Kim DW, Rhee HW (2002) Bull Korean Chem Soc 23:683
17. Vogel H (1922) Z Phys 22:645
18. Tamman VG, Hesse HG (1926) Anorg Allg Chem 19:245
19. Fulcher GS (1925) J Am Ceram Soc 8:339
20. Saikia D, Kumar A, Singh F, Avasthi DK (2006) J Phys D Appl Phys 39:4208
21. Appetecchi GB, Romagnoli P, Scrosati B (2001) Electrochem Commun 3:281
22. Padhi AK, Nanjundaswamy KS, Goodenough JB (1997) J Electrochem Soc 144:1188
23. Franger S, Le Cras F, Bourbon C, Rouault H (2003) J Power Sources 119–121:252
24. Yamada A, Chung SC, Hinokuma K (2001) J Electrochem Soc 148:A224
25. Andersson AS, Thomas JO (2001) J Power Sources 97–98:498
26. Streltsov VA, Belokoneva EL, Tsirelson VG, Hansen NK (1993) Acta Cryst B49:147
27. Geller S, Durand JL (1960) Acta Cryst 13:325
28. Hassoun J, Panero S, Mulas G, Scrosati B (2007) J Power Sources 171:928